SPECIAL CORE ANALYSIS STUDIES IN VUGGY POROUS MEDIA OF CONTROLLED MICROSTRUCTURE

G.S. Padhy, M.A. Ioannidis, C. Lemaire
University of Waterloo, Canada

ABSTRACT

The pore microstructure of carbonates is vastly more complex than siliciclastic rocks due to diverse post-depositional diagenetic processes. These processes are responsible for the development of porosity at multiple scales, as is the case for vuggy carbonates. Progress in the modeling of the petrophysical properties of vuggy carbonates is complicated by the relative absence of experiments in systems of controlled microstructure. In an attempt to remedy this situation, the task is undertaken of synthesizing and characterizing model porous media with well-controlled vuggy and matrix porosity. These media are created by mixing monodispersed glass beads and calcium carbonate particles of different known sizes in known proportions, consolidating the mixture in an oven and then dissolving the carbonate particles by flowing acid. We report on the synthesis of these model vuggy media and on the results of a comprehensive petrophysical characterization that includes measurements of their porosity, permeability, capillary and electrical properties and pore size distribution by thin section imaging and NMR/MRI methods.

INTRODUCTION

Recent studies have focused on modeling the capillary, flow and electrical properties of vuggy carbonates using pore network models or stochastic reconstruction techniques [1-5]. These studies have sought to account for the effect of the microstructure at two different scales, corresponding to vug and matrix pores, but validation of their results has been hampered by the lack of experimental data on systems with well characterized matrix and vuggy porosity. The synthesis of such systems is described below.

Sample Preparation

The vuggy media were prepared by mixing glass beads and $CaCO_3$ particles of widely different, but known size. The size contrast between glass beads and $CaCO_3$ particles was one order of magnitude, so as to obtain a clear size contrast between vugs and matrix pores. Desired proportions (to control vug porosity) of glass beads and $CaCO_3$ particles were mixed and packed in a crucible for sintering. The mixture was sintered for 1hr at different temperatures ranging from 680°C to 715°C to achieve good consolidation of the glass beads and control of the total porosity. Core plugs of 3.8cm diameter and about 5 cm length were drilled and dried. The vugs in the plugs were created by first soaking the plugs in dilute HCl for few hrs and then flushing them with copious amounts of dilute

HCl to dissolve $CaCO_3$ completely. Thereafter, the plugs were flushed with many pore volumes of de-ionized water and sonicated to remove any precipitated particles.

EXPERIMENTAL APPROACH, RESULTS AND DISCUSSION

Porosity and Permeability

The total porosity of the samples was determined by a saturation method and the vug porosity (ϕ_v) and matrix porosity (ϕ_m) were calculated using the following relations:

$$\phi_v = \frac{\phi - \phi_m}{1 - \phi_m} \; , \; \phi_v = \frac{V_v}{V_b} \tag{1}$$

In Eq. (1), V_v is the vug volume, determined from the weight and bulk density of $CaCO_3$ particles, V_b is the bulk volume and ϕ is the total porosity of the sample.

The Klinkenberg-corrected permeability to air for all samples was measured before ($k_s^{(p)}$) and after ($k_s^{(v)}$) dissolution of the $CaCO_3$ particles. Porosity and permeability measurements are summarized in Table 1. These measurements were used to test the applicability of the following expression, obtained by combining the analytical results of Neale et al. [6] for uniform systems containing voids or impermeable inclusions:

$$\frac{k_s^{(v)}}{k_s^{(p)}} = \frac{(1 + 2\phi_v)(2 + \phi_v)}{2(1 - \phi_v)^2} \tag{2}$$

As seen in Figure 1, the prediction of Neal et $al.$ is within a factor of two of the experimental data for $\phi_v < 0.2$ and within a factor of three for $\phi_v > 0.2$. The deviation from experimental data increases with increasing vug porosity, that is, as the probability of local vug percolation (touching vugs) increases.

Electrical Properties

An in-$house$ designed four-electrode system was used for electrical measurements. The sample was saturated using a 30,000ppm NaCl solution and placed in a sleeve under 400 psi overburden pressure and equipped with a 0.2µm hydrophilic membrane at the exit face to prevent breakthrough of the injected non-wetting phase. The core holder was placed vertically and the sample was desaturated by continuously injecting humidified air at a rate of 0.033cc/min using a constant rate high-pressure pump. The average brine saturation was determined continuously by a gravimetric method. Electric impedance was measured using an AC voltage of 1V at a frequency of 30 kHz. Saturation and impedance measurements were recorded simultaneously at fixed time intervals by a data acquisition system. A pressure transducer was also attached at the inlet to monitor the pressure of injected gas and ensure that the non-wetting phase had not exited the system.

A Berea sample ($\phi = 22.3\%$) was measured first to test the reliability and accuracy of the design. The cementation exponent (m) and saturation exponent (n) were calculated using Archie's equations and were found to be 1.90 and 1.99 (+/-0.09) respectively, in good agreement with literature values. Next, electrical measurements were conducted in

vuggy samples and repeated in triplicate to ascertain reproducibility. The data for two samples are presented in Figure 2 and Table 2. For both samples, a flattening out of the resistivity index (RI) with decreasing water saturation is observed at the lowest levels of water saturation, where resistivity is dominated by thin water layers connecting pendular rings and thus becomes insensitive to saturation changes.

Mercury Intrusion Porosimetry (MIP)
MIP measurements were performed on small cylindrical representative samples in two stages, namely low pressure (~1psi to 50psi) and high pressure (20 psi to 40000psi) and the result for one sample (SC 4a) is shown in Figure 3. Mercury intrusion reveals that the majority of pore volume is accessible through pore throats in the range 50-70 μm in diameter, whereas mercury extrusion indicates that most pores from which mercury retracts have a diameter in the range 100-200 μm. MIP and saturation porosity agree with each other. However, there is a slight difference in comparison to the whole sample, which is ascribed to sample heterogeneity (Table 3).

Breakthrough Capillary Pressure and Capillary Pressure

Breakthrough capillary pressure (P_c^o) was measured on brine saturated core plugs by injecting air at a very low constant rate of 0.033cc/min. The pressure trace was continuously recorded via an acquisition system and the highest pressure recorded was considered as the P_c^o (Figure 4a). The result was compared with the pressure trace obtained during electrical measurement (Figure 4b). Good agreement between the two was found. The values of P_c^o for all samples are given in Table 1.Comparison of the air-brine capillary pressure and MIP data (after scaling of the former using $\gamma_{wa} = 0.070$N/m, $\gamma_{ma} = 0.485$N/m, $\theta_{wa} = 0°$ and $\theta_{ma} = 150°$) revealed differences in capillary pressure values of approximately a factor of two (Figure 5). This difference was attributed to sample heterogeneity and difference in sample volume under consideration (i.e. whole plug in air-water case vs. a small piece in MIP case).

Thin Section Imaging
Digital images (16000 x 12000 pixels) from over sized thin sections (3.8cm diameter) as well as backscatter SEM images (Fig. 6) were acquired. These images reveal three families of pores: vugs (molds of dissolved calcium carbonate particles), pores between closely packed glass beads and pores associated with flaws in the glass bead packing.

Nuclear Magnetic Resonance and Magnetic Resonance Imaging
NMR/MRI studies were performed on a cylindrical sample of size 0.8cm x 0.8cm, taken from plug SC 4a. The sample was tightly placed inside a Teflon cup, evacuated and saturated with de-ionized water. Reference water was placed on top of the sample. High-resolution (187x187x374μm^3 voxel) 1D, 2D and 3D images were acquired to provide information about the spatial distribution of vugs, matrix pores and their contribution towards total porosity. Total porosity and porosity distribution were also obtained from

computed density images. The computed porosity agrees with the saturation porosity (ϕ = 47.02%) measured on this sample. 3D MRI images of the sample under full and partial (vugs drained) saturation conditions are presented in Figure 7.

Pore size distribution measurements were made using the DDIF method (decay due to diffusion in the internal magnetic field) developed by Song [7]. The internal magnetic field represents the pore geometry of a fully saturated as well as partially saturated media. In this method the pore diameter is related to the relaxation time τ according to, $d = \pi\sqrt{D\tau}$, where d is the pore diameter in μm, D is the bulk diffusion constant = 2×10^{-9} m^2/s. The relaxation data were fitted via a multi exponential fitting procedure and a relaxation time distribution was obtained. The pore size distributions resulting from these calculations were mostly bimodal and ranging from 10μm to 250μm as shown in Figure 8. As evident from Figure 8 the matrix pores range from 10μm to 185μm and the rest is attributed to the distribution on vugs (size 1.18mm-2.38mm). The vug size distribution could not be obtained, as the relaxation time for bulk water is 3μs, corresponding to a maximum detectable pore size of 243 μm. However, their presence is seen collectively in the NMR signal associated with pores greater than about 185 μm, resulting in an estimate of their contribution towards the total porosity in good agreement with independently determined values (Table 1).

CONCLUSION
Special core analysis measurements done on model vuggy media of controlled microstructure have the potential to become a basis for better understanding SCAL results on vuggy carbonates and for improving and validating microstructure models for porous media containing porosity at multiple scales.

REFERENCES
1. Ioannidis, M.A., Kwiecien, M.J. and Chatzis, I., Electrical Conductivity and Percolation Aspects of Statistically Homogeneous Porous Media. *Transport in Porous Media*, (1997) **29**, 61-83.
2. Ioannidis, M.A. and Chatzis, I., A Dual-Network Model of Pore Structure for Vuggy Carbonates, *Proceedings of the Annual Symposium of the Society of Core Analysts*, (2000), October, Abu-Dhabi, U.A.E.
3. Moctezuma, A., Bekri, S., Laroche, C. and Vizika, O., A Dual-Network Model for Relative Permeability of Bimodal Rocks: Application in a Vuggy Carbonate. *Proceedings of the Annual Symposium of the Society of Core Analysts*, (2003), September, Pau, France.
4. Moctezuma-Berthier, A., Vizika, O. and Adler, P.M., Macroscopic Conductivity of Vugular Porous Media. *Transport in Porous Media*, (2003) **49**, 313-332.
5. Moctezuma-Berthier, A., Vizika, O., Thovert, J.-F. and Adler, P.M., One- and Two-Phase Permeabilities of Vugular Porous Media. *Transport in Porous Media*, (2004) **56**, 225-244.

6. Neal, G., Anaka, H. and Hampel, D., Transport Phenomena in Non-Homogeneous Porous Media: Fluid Flow. *The Canadian Journal of Chemical Engineering*, (1975) **53**, 691-694.
7. Song, Y.Q., Pore sizes and pore connectivity in rocks using the effect of internal field, *Magnetic Resonance Imaging*, (2001) **19**, 178-421.

Table 1. Petrophysical data of model vuggy media.

Sample	Bead Size (μm)	Vug Size (mm)	ϕ	ϕ_v	$k_s^{(p)}$ (mD)	$k_s^{(v)}$ (mD)	$k_s^{(p)}/k_s^{(v)}$	P_c^o (psi)
SC-3a	75-100	1.18-2.38	0.4225	0.1194	900.00	2050.00	0.4390	0.767
SC-4a	125-150	1.18-2.38	0.4832	0.1404	5400.00	7140.00	0.7563	0.203
SC-4b	125-150	1.18-2.38	0.4683	0.1242	3390.00	4740.00	0.7152	0.387
SC-5a	125-150	1.18-2.38	0.4276	0.1576	5050.00	8240.00	0.6129	0.312
SC-5b	125-150	1.18-2.38	0.4377	0.1681	3250.00	3690.00	0.8808	0.557
SC-7a	125-150	1.18-2.38	0.4670	0.1702	12050.00	23340.00	0.5163	N/A
SC-8a	125-150	1.18-2.38	0.3109	0.1981	4070.00	8050.00	0.5056	0.092
SC-11a	75-63	1.18-2.38	0.2471	0.2243	141.87	1552.10	0.0914	0.212
SC-16a	75-63	0.841-1.18	0.3208	0.2516	207.05	2406.00	0.0861	0.200
SC-17a	75-63	0.841-1.18	0.4797	0.3688	1193.50	9450.00	0.1263	0.192

Table 2. Comparison of 'm' and 'n' values of SC 4a and SC 4b samples.

Trial		SC 4a		SC 4b
	m	n	m	n
1st	1.29	2.27(+/-0.07)	1.47	1.76(+/-0.02)
2nd	1.32	2.31(+/-0.02)	1.45	1.88(+/-0.02)
3rd	1.33	2.28(+/-0.02)		

Table 3. Comparison of porosity estimates.

Sample	ϕ		
	Saturation (whole plug)	MIP (small piece)	Saturation (small piece)
SC4a	0.4832	0.4696	0.463
SC4b	0.4683	0.4586	0.4488
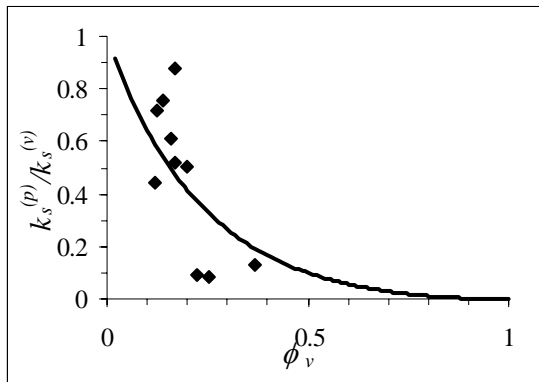
Figure 1. Permeability enhancement due to vugs, experiment (♦), Neale *et al.* (-)
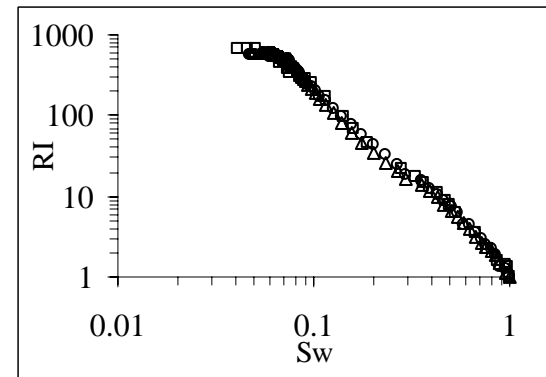
Figure 2. Resistivity index plot of SC 4a; comparison of 3 trials, 1st (□), 2nd (△), 3rd (○)
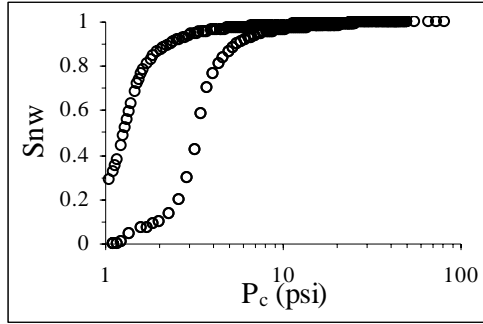
Figure 3. MIP drainage and imbibition capillary pressure curves of sample SC4a
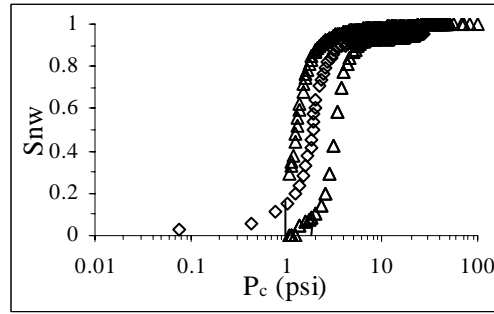
Figure 5. Comparison of capillary pressure curves, Hg-air (△) and air-water (scaled) (◇)
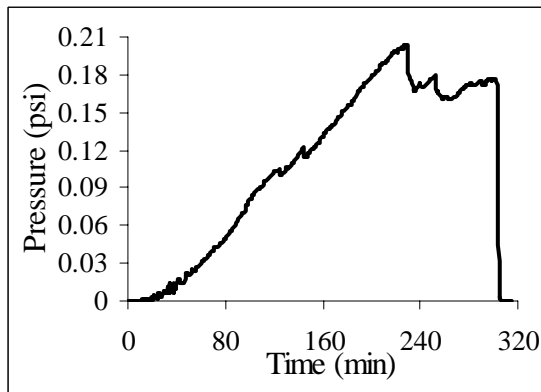
Figure 4a. Breakthrough capillary pressure (= 0.203psi) trace of sample SC 4a.
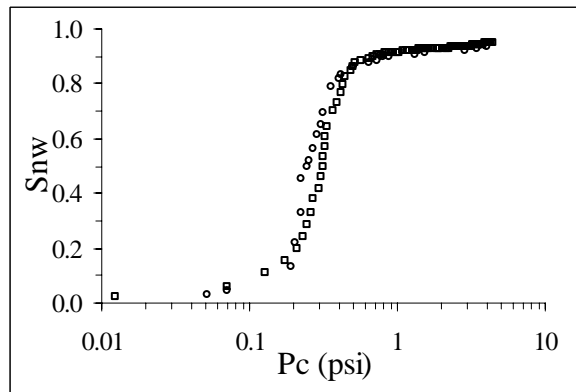
Figure 4b. Pressure trace of SC 4a during electrical measurement (repeat experiments)
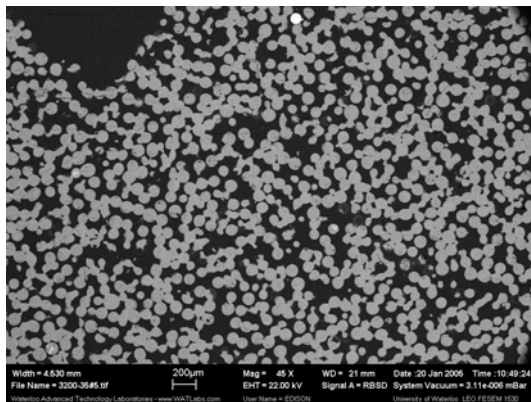
Figure 6. BSEM image of sample SC 4a.
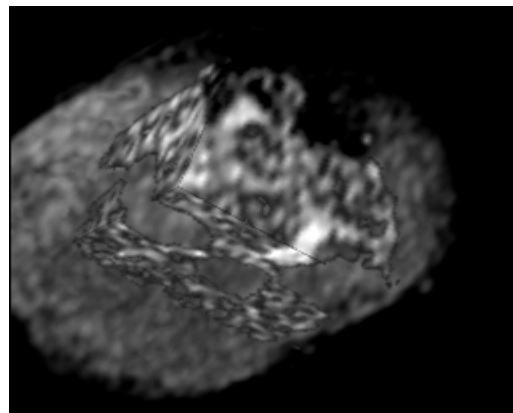
Figure 7. 3D MRI of partially saturated sample SC 4a, (white: water-filled pores, black: solid grains/drained pores)
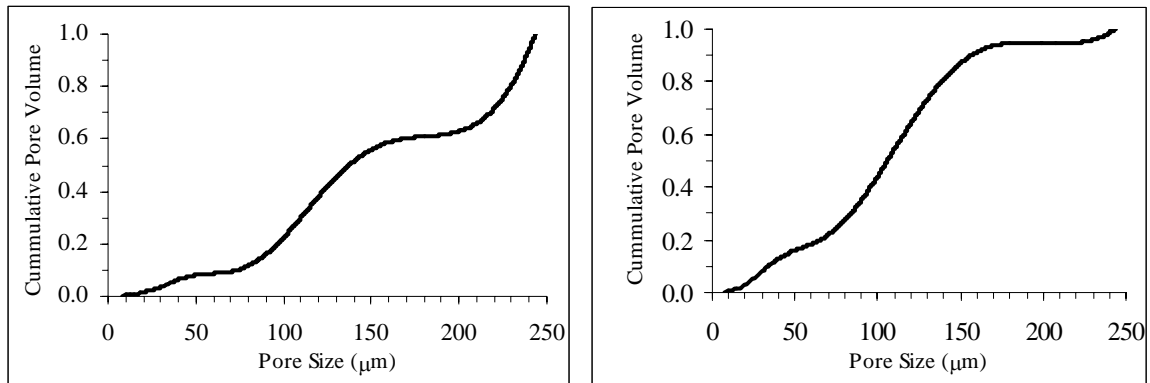
Figure 8. Cumulative pore size distribution of sample SC 4a, under conditions of full (left) and partial saturation (drained vugs; right) from NMR.